

UCLA

UCLA Previously Published Works

Title

Characterization of ventromedial hypothalamus activity during exposure to innate and conditioned threats

Permalink

<https://escholarship.org/uc/item/0v82p8f9>

Journal

European Journal of Neuroscience, 57(7)

ISSN

0953-816X

Authors

Tobias, Brooke C
Schuette, Peter J
Maesta-Pereira, Sandra
[et al.](#)

Publication Date

2023-04-01

DOI



10.1111/ejn.15937

Copyright Information

This work is made available under the terms of a Creative Commons Attribution-NonCommercial-NoDerivatives License, available at <https://creativecommons.org/licenses/by-nc-nd/4.0/>

Peer reviewed

Characterization of ventromedial hypothalamus activity during exposure to innate and conditioned threats

Brooke C. Tobias | Peter J. Schuette | Sandra Maesta-Pereira  | Anita Torossian | Weisheng Wang | Ekayana Sethi | Avishek Adhikari 

Department of Psychology, University of California, Los Angeles, Los Angeles, CA, USA

Correspondence

Avishek Adhikari, Department of Psychology, University of California, Los Angeles, Los Angeles, CA 90095, USA.
Email: avi@psych.ucla.edu

Funding information

National Institute of Mental Health, Grant/Award Numbers: R00 MH106649, R01 MH119089; Brain and Behavior Research Foundation, Grant/Award Numbers: 22663, 27780; National Science Foundation, Grant/Award Number: NSF-GRFP DGE-1650604; UCLA Affiliates Fellowship; Hellman Foundation

Edited by: Camilla Bellone.

Abstract

In the face of imminent predatory danger, animals quickly detect the threat and mobilize key survival defensive actions, such as escape and freezing. The dorsomedial portion of the ventromedial hypothalamus (VMH) is a central node in innate and conditioned predator-induced defensive behaviours. Prior studies have shown that activity of steroidogenic factor 1 (sf1)-expressing VMH cells is necessary for such defensive behaviours. However, sf1-VMH neural activity during exposure to predatory threats has not been well characterized. Here, we use single-cell recordings of calcium transients from VMH cells in male and female mice. We show this region is activated by threat proximity and that it encodes future occurrence of escape but not freezing. Our data also show that VMH cells encoded proximity of an innate predatory threat but not a fear-conditioned shock grid. Furthermore, chemogenetic activation of the VMH increases avoidance of innate threats, such as open spaces and a live predator. This manipulation also increased freezing towards the predator, without altering defensive behaviours induced by a shock grid. Lastly, we show that optogenetic VMH activation recruited a broad swath of regions, suggestive of widespread changes in neural defensive state. Taken together, these data reveal the neural dynamics of the VMH during predator exposure and further highlight its role as a critical component of the hypothalamic predator defense system.

1 | INTRODUCTION

Predators are a major source of lethal danger for a wide variety of animals. Consequently, animals have specialized circuits dedicated to detecting predators and to

rapidly evading this danger (Martinez et al., 2008). Recent evidence has indicated that a critical node of predator-induced defense is located in the medial hypothalamus. This circuit consists of the dorsomedial pre-mammillary nucleus, the anterior hypothalamus and the

Abbreviations: AAV, adeno associated virus; ChR2, channelrhodopsin 2; CNO, clozapine-N-oxide; DIO, double floxed inverted open reading frame; Efla, elongation factor 1 alpha; GLM, generalized linear model; GRIN, gradient index; IRES, internal ribosomal entry site; VMH, ventromedial hypothalamus; Sf1, steroidogenic factor 1.

dorsomedial portion of the ventromedial hypothalamus (VMH). These three structures show intense activation induced by exposure to predators, as measured by *cfos* expression (Faturi et al., 2014; Martinez et al., 2008; Silva et al., 2013). Additionally, all three regions produce defensive behaviours during optogenetic activation. For example, optogenetic activation of the dorsal premammillary nucleus and the anterior hypothalamus produce robust escape, even in the absence of threat (Wang et al., 2015; Wang, Schuette, La-Vu, et al., 2021). Recently, activation of the anterior hypothalamus has also been shown to induce defensive attacks (Xie et al., 2022). In contrast, optogenetic activation of steroidogenic factor 1 (*sf1*)-expressing glutamatergic VMH cells produces freezing, escape and avoidance of open spaces (Kunwar et al., 2015; Wang et al., 2015). These three hypothalamic nuclei are robustly interconnected (Canteras & Swanson, 1992; Comoli et al., 2000), and prior anatomical and functional evidence indicates these nuclei produce defensive behaviours by projections to the brainstem periaqueductal grey region (Beitz, 1982; Wang et al., 2015; Wang, Schuette, La-Vu, et al., 2021; Xie et al., 2022). These hypothalamic structures have thus been named the hypothalamic predator defense system (Martinez et al., 2008).

It is known that the VMH and other members of this circuit are activated by predator or predator cues (Martinez et al., 2008; Silva et al., 2013). Indeed, the dorsal premammillary nucleus has been reported to encode a wide variety of relevant defensive metrics, including distance to predator and activation prior to escape (Wang, Schuette, La-Vu, et al., 2021; Wang, Schuette, Nagai, et al., 2021). However, the neural dynamics of *sf1* VMH cells during predator exposure remains relatively uncharacterized. Recent work has shown that VMH cells in mice are active during flight (Esteban Masferrer et al., 2020) and these cells show persistent activation following exposure to a predatory rat (Kennedy et al., 2020), suggesting they may induce a defense-related emotional state (Kunwar et al., 2015; Kennedy et al., 2020). However, answers to important issues remain unknown. Do these cells represent or predict the future occurrence of defensive behaviours? How do VMH *sf1* cells encode distance to conditioned threats such as a shock grid?

Here, we address these questions by obtaining neural recordings from VMH cells. We show that VMH cells were more active during proximity to innate predatory threats but not a fear-conditioned shock grid or a control stimulus such as a toy rat. The activity of VMH cells could also be used to predict the occurrence of future escape but not freezing.

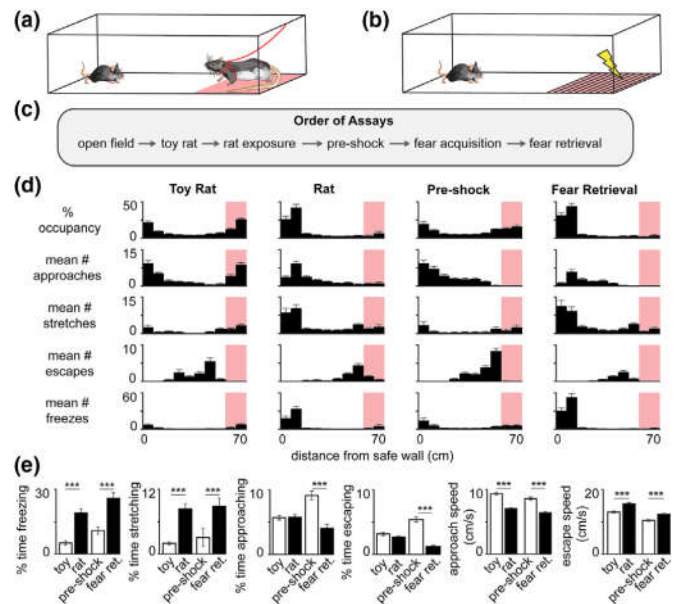
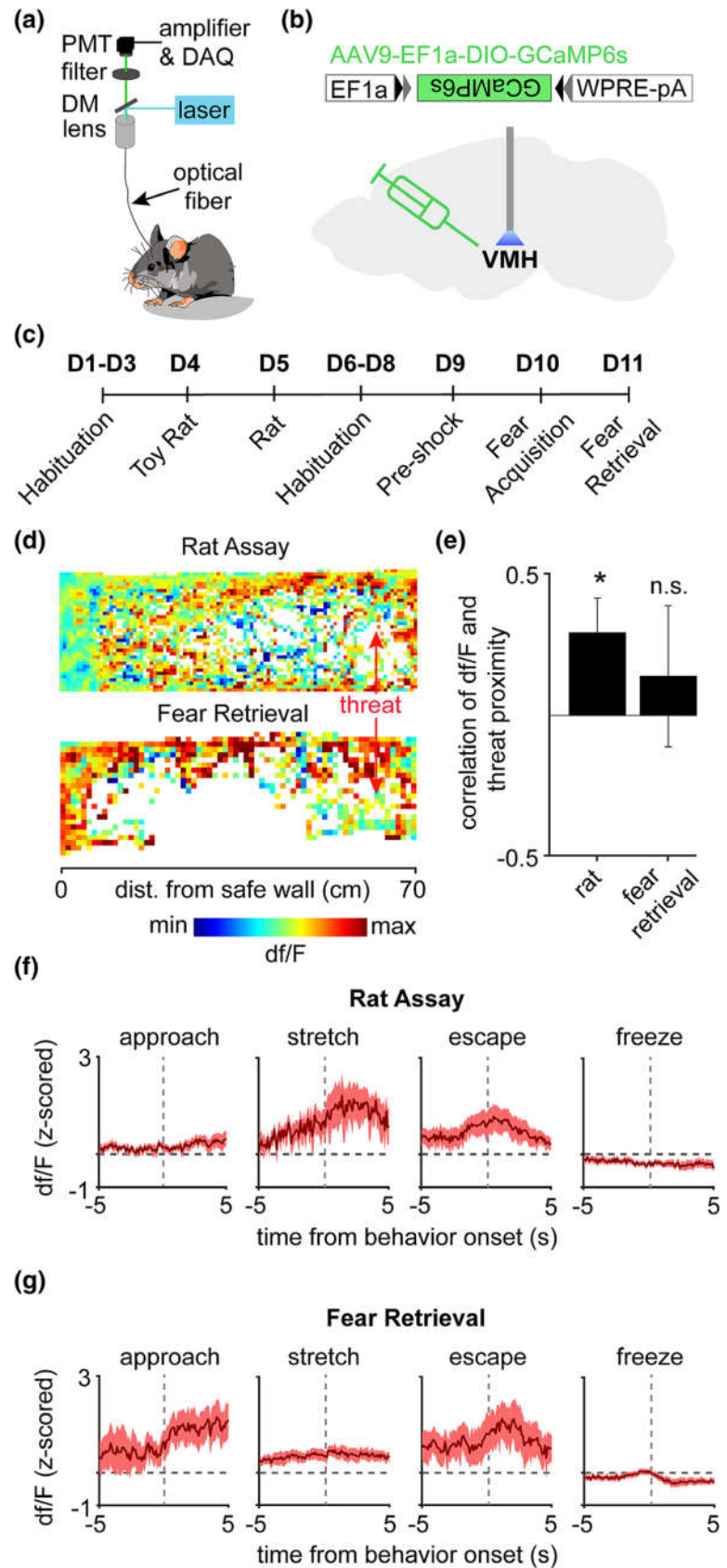


FIGURE 1 Rat and fear conditioning assay characterization. (a, b) Diagrams of the rat and fear conditioning assays. (c) Summary of the behavioral timeline. (d) Histograms show the distribution of behaviors across the length of the enclosure for each assay (toy rat $n = 16$, rat $n = 36$, pre-shock $n = 27$ and fear retrieval $n = 32$). (e) Bars represent the mean % time freezing, stretching, approaching and escaping as well as the mean approach and escape speed for toy rat/rat and pre-shock/fear retrieval assays (Wilcoxon rank sum test; same n as d). *** $p < .001$

Prior data with optogenetic activation of VMH-*sf1* cells have shown that these cells produce a variety of defensive behaviours (Kunwar et al., 2015; Wang et al., 2015). However, optogenetic activation produces unnatural and synchronous activation of cells, which does not resemble endogenous neural dynamics. Thus, to address if more naturalistic activation patterns also induce defensive behaviours, we studied the effect of chemogenetic activation of VMH *sf1* cells. This manipulation increased freezing and avoidance of a live predator but not of a fear-conditioned shock grid, indicating VMH *sf1* activity is sufficient to generate robust defense against innate predatory threats but not conditioned threats. Lastly, we show that optogenetic activation of VMH-*sf1* cells induces *cfos* expression in a wide variety of targets, demonstrating recruitment of a distributed hypothalamic-brainstem defensive network.

These data complement prior work, indicating the VMH is a vital structure mediating defense to innate but not conditioned threats, in agreement with prior reports (Cezario et al., 2008; Martinez et al., 2008; Silva et al., 2013), and provide insights on how the neural dynamics of this region are used to generate rapid evasive manoeuvres to minimize the danger of predators.

FIGURE 2 (a) Scheme shows setup used for fibre photometry recording. (b) VMH was targeted with AAV9-EF1a-DIO-GCaMP6s. (c) Diagram shows the order of assays across days (abbreviated as 'D'). (d) Average heat maps of enclosures, viewed from above, show that VMH sf1 cells are more active closer to threat in the rat assay but not in the fear retrieval assay (rat $n = 6$; fear retrieval $n = 5$). White squares represent unvisited regions, and warmer colours represent higher VMH sf1 neural activity. The maps are averaged across mice ($n = 6$). (e) Bars show the mean Spearman correlation of df/F and threat proximity (Wilcoxon signed rank test; n same as d). (f) Behaviour-triggered average showing mean VMH activity during approach to rat, stretch-attend postures, escape from rat and freeze (mouse $n = 6$; rat behaviour counts: approach $n = 71$, stretch $n = 118$, escape $n = 59$ and freeze $n = 159$). (g) Same as (f) but for the fear retrieval assay (mouse $n = 5$; fear retrieval behavior counts: approach $n = 13$, stretch $n = 35$, escape $n = 12$ and freeze $n = 264$). $*p < .05$



2 | RESULTS

2.1 | Characterization of predator and shock grid assays

In order to study the role of VMH sf1 cells in defense, we exposed mice to either a predatory rat or a shock grid, as we have done previously (Figure 1a,b). During the rat assay, mice were exposed for 20 min to either a control toy rat or a live rat. The live rat was restrained by a harness and could only explore the area highlighted in red (Figure 1a). For the shock grid assay, mice first explored the environment in the absence of shock (pre-shock control assay). Twenty-four hours later, on the fear acquisition day, they received a foot shock whenever they touched the shock grid located at the end of the corridor. The next day (fear retrieval), conditioned responses to the shock grid were measured.

Both the rat and the shock grid assays induced a rich ethogram of defensive behaviours including freezing, escape, risk-assessment stretch-attend postures and threat avoidance (Figure 1d). Importantly, the spatial distribution of these behaviours is in agreement with the framework elaborated by the predatory imminence continuum theory (Perusini & Fanselow, 2015), which posits that mice escape from predators during close encounters and that they freeze at larger distances to avoid visual detection by the predator. Accordingly, we observed that escape occurs closer to the threat, while freezing was displayed at larger distances from threat (Figure 1d). Furthermore, relative to a control stimulus, mice approached threats more slowly and escaped with high velocity, indicating cautious exploratory approach and vigorous flight (Figure 1e). All defensive behaviours were displayed more frequently during exposure to threat compared to control toy rat and pre-shock assays (Figure 1d,e). No sex differences were observed in any defensive measure (Figure S1). Taken together, these data indicate that the rat and conditioned shock grid assays both induced naturalistic defensive behaviours.

We next investigated the population neural dynamics of VMH sf1 cells during exposure to these assays with a sf1 cre line, as done previously (Kunwar et al., 2015; Wang et al., 2015; Zhang et al., 2020). To do so, we infused the cre-dependent vector AAV9-EF1a-DIO-GCaMP6s in the VMH of sf1-cre mice and used fibre photometry to record calcium transients via the genetically encoded fluorescent calcium indicator GCaMP6s (Figure 2a,b). Heat maps of neural activity indicated that VMH sf1 cells were activated by proximity to the rat but not the shock grid (Figure 2d), even though both assays induced comparable frequency and intensity of defensive behaviours (Figure 1). To quantify this effect, we

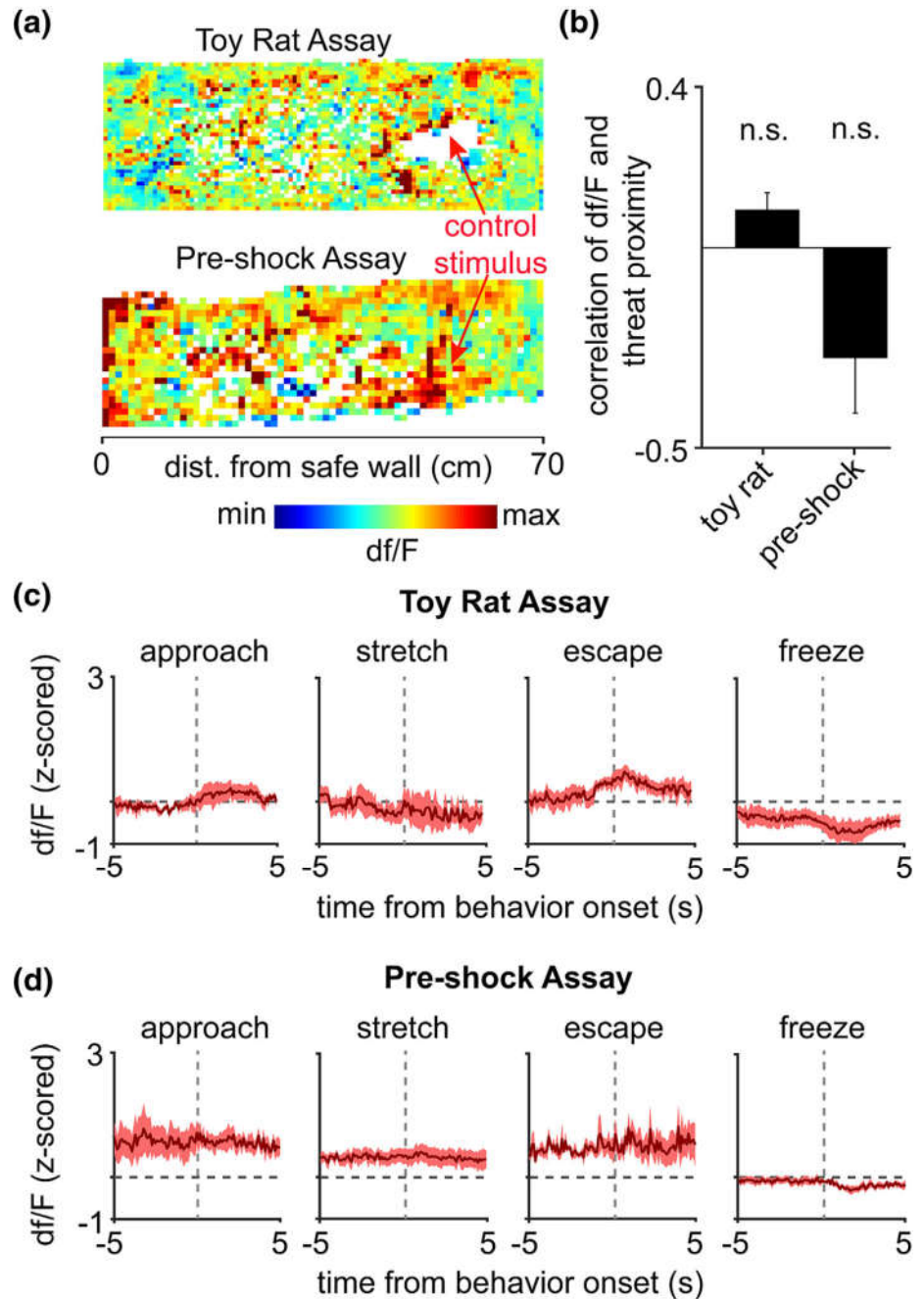
calculated the correlation between neural activity (measured as fluorescence df/F) and threat proximity. VMH neural activity was significantly correlated with rat proximity but not with distance to shock grid (Figure 2e). We also characterized population activity during defensive behaviours and observed that significant increases in activity were seen only during escape in the rat assay (Figure S2), in agreement with prior data showing VMH sf1 activation induces escape-related actions (Kunwar et al., 2015; Wang et al., 2015).

Importantly, VMH activity did not correlate with proximity to control stimuli, such as a toy rat and the shock grid prior in the pre-shock day (Figure 3a,b). Robust activation was also not seen during escape movements away from these control stimuli (Figure 3c,d). These data indicate that VMH population activity represents proximity to a predator and is active during escape from threats.

2.2 | VMH sf1 cells encode flight and distance to a live predator

We then studied the neural dynamics of the VMH with single-cell resolution. We thus implanted a miniaturized microscope to image GCaMP6s-expressing VMH sf1 cells (Figure 4a) and proceeded to record calcium transients in these cells (Figure 4b). We observed that VMH cells were activated with diverse temporal profiles around approach, stretch-attend, escape and freeze during exposure to both threat assays (Figure 4c). We then constructed generalized linear models (GLMs) and calculated GLM weights for each cell and each of the four behaviours above. We circularly shifted the neural data over 100 iterations and recalculated the GLM weights for each cell, building a shuffled distribution. Cells for which the actual GLM weight for a particular behaviour was larger than the 95th percentile of the shuffled distribution were classified as significantly encoding that particular behaviour (see Section 4). This was done during exposure to both threats and control assays. In the rat assay, relative to the toy rat exposure, a larger fraction of behaviour-modulated cells was observed for stretch-attend postures and for escape (Figure 4d). In the fear retrieval assay, a significantly larger fraction of modulated cells than in pre-shock was only observed for cells encoding stretch-attend postures (Figure 4d). We then used logistic regression to decode the occurrence of the measured behaviours in both control and threat assays. The only behaviour that could be decoded significantly above chance was escape, which could be decoded in both threat assays but not in control assays (Figure 4e). We next asked if VMH activity could be used to predict

FIGURE 3 (a) Average heat maps of enclosures, viewed from above, show that VMH cells are not more active closer to control stimulus (toy rat $n = 6$; pre-shock $n = 5$). White squares represent unvisited regions. (b) Bars show the mean Spearman correlation of df/F and control stimulus proximity (Wilcoxon signed rank test; n same as a). (c) Behaviour-triggered average showing mean VMH activity during approach to toy rat, stretch-attend postures, escape-like movements from toy rat and freeze (mouse $n = 6$; toy rat behavior counts: approach $n = 58$, stretch $n = 75$, escape $n = 38$ and freeze $n = 104$). (d) Same as (c) but for the pre-shock assay (mouse $n = 5$; shock habituation behaviour counts: approach $n = 41$, stretch $n = 32$, escape $n = 23$ and freeze $n = 134$)



the future occurrence of escape. Prediction of future displays of other behaviours was not performed since the other three behaviours could not be decoded by VMH activity (Figure 4e). Intriguingly, VMH sf1 activity could be used to predict escape occurrence up to 2 s prior to the onset of escape in both assays (Figure 4f). We also investigated if VMH neural activity could be used to predict escape using unsupervised methods. To do so, we performed k-means clustering on the top principal components of VMH activity that accounted for 80% of the variance. No information about behaviour was provided to the model. We performed the simplest iteration of this model, which is performing k-means clustering using

two clusters, to separate the neural ensemble activity into either of two states. Representative data showing the output of the model indicate that different time points of ensemble activity were classified into two states (Figure 4g, black traces). We then plotted time points in which escapes occurred on top of the model output (Figure 4g, light red boxes) and observed that escapes could be well predicted by the unsupervised model output. Intriguingly, this simple unsupervised analysis was able to predict the occurrence of escape with an accuracy higher than chance (Figure 4h). These data indicate that escape-related neural activity is a prominent feature of VMH sf1 cells.

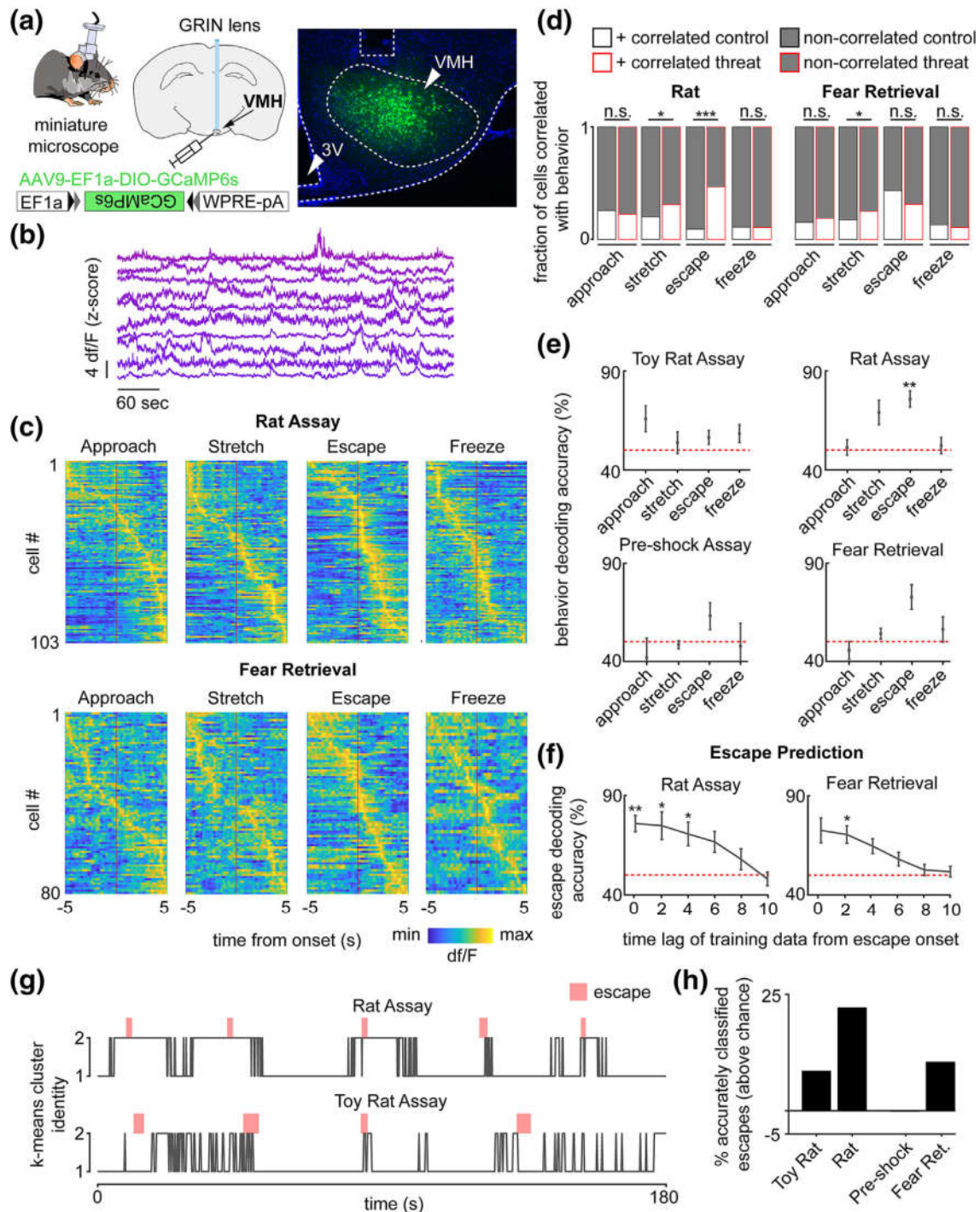


FIGURE 4 Legend on next page.

2.3 | VMH sf1 chemogenetic activation increases threat avoidance and freezing

Next, we activated VMH sf1 cells to observe if this manipulation was sufficient to increase defensive behaviours. We activated VMH sf1 cells chemogenetically, by expressing the excitatory receptor hM3Dq in these cells

(Figure 5a). Chemogenetic excitation of VMH sf1 cells increased avoidance of the centre of the open field, which is commonly used as a measure of anxiety in rodents (Figure 5c). This manipulation also increased freezing and entries in the rat zone during the rat exposure assay (Figure 5d). However, no effects were seen in the fear retrieval day of the shock grid assay (Figure 5d),

FIGURE 4 (a, left) *sfl* cre mice were injected with AAV9-EF1a-DIO-GCaMP6s in the VMH and then were implanted with a miniaturized microscope. (a, right) Example histology. (b) Calcium transients of a representative subset of GCaMP6s-expressing VMH cells recorded in a single session. (c) Colour maps of average df/F for all recorded VMH cells aligned to each scored behavior in the rat (top) and shock grid fear retrieval (bottom) assays. Cells are ordered by peak activation. (d) Bars indicate the fraction of cells that were categorized as being either positively correlated or non-correlated with each classified behaviour, for threat and control assays. More cells were significantly correlated with escape from rat than escape from toy rat. This measure did not significantly differ from pre-shock to fear retrieval sessions (Fisher's exact test; rat assay: approach + $n = 23$, non-correlated $n = 70$, stretch + $n = 32$, non-correlated $n = 49$, escape + $n = 48$, non-correlated $n = 41$, freeze + $n = 11$, non-correlated $n = 60$, toy rat assay: Approach + $n = 28$, non-correlated $n = 57$, stretch + $n = 22$, non-correlated $n = 67$, escape + $n = 10$, non-correlated $n = 43$, freeze + $n = 12$, non-correlated $n = 47$, pre-shock assay: approach + $n = 7$, non-correlated $n = 49$, stretch + $n = 8$, non-correlated $n = 43$, escape + $n = 20$, non-correlated $n = 39$, freeze + $n = 6$, non-correlated $n = 48$, fear retrieval assay: Approach + $n = 15$, non-correlated $n = 46$, stretch + $n = 20$, non-correlated $n = 36$, escape + $n = 25$, non-correlated $n = 40$, freeze + $n = 9$, non-correlated $n = 36$). (e) Only escape can be decoded by VMH cell activity in the rat (top) and shock grid fear retrieval assays (bottom) (one-sample t test; toy rat assay $n = 5$, rat assay $n = 4$, preshock assay $n = 3$, fear retrieval assay $n = 3$). (f) VMH cell activity can predict escape from threat prior to escape onset (one-sample t test; n same as in e). (g) Clusters were extracted from the neural data (k -means, $k = 2$). For these examples, the clusters (grey) successfully separate escape from non-escape epochs for the rat assay (top) but not for the toy rat assay (bottom). (h) Bars indicate the percent of accurately classified escapes, by k -means, above chance level. *** $p < .001$, ** $p < .01$, * $p < .05$, † $p = .07$

indicating that VMH activation is sufficient to increase defense to a predatory innate threat but not to a conditioned shock grid threat. Lastly, no sex differences were seen in the rat assay (Figure S3), and chemogenetic effects in the open field and rat assay were not correlated across mice (Figure S4).

2.4 | VMH *sfl* optogenetic activation recruits defensive nodes

Lastly, we investigated which downstream circuits may be activated during strong activation of VMH *sfl* cells. To do so, we expressed the excitatory opsin ChR2 in VMH *sfl* cells (Figure 6a) and then exposed mice to an open field for 10 min. Mice received unilateral optogenetic stimulation of VMH cells (20 Hz, 5-ms pulse train) during this time and then were transcardially perfused 90 min later. We processed the tissue and performed immunocytochemistry using anti *cfos* antibodies to quantify the recruitment of brain regions due to VMH activation. Increased *cfos* expression was mostly observed in regions known to receive direct VMH innervation, such as the periaqueductal grey and the dorsal premammillary nucleus, indicating that VMH activation can recruit regions known to control defensive actions (Figure 6c). We also observed that optogenetic activation of VMH *sfl* cells increases freezing (Figure S5), as reported previously (Wang et al., 2015).

3 | DISCUSSION

Here, we show that VMH *sfl* cells encode distance to an innate predatory threat but not to a fear conditioned

shock grid or to control stimuli such as a toy rat. Our data also show that VMH activity can predict future occurrence of escape but not other defensive behaviours. Furthermore, chemogenetic activation of VMH *sfl* cells increases avoidance of open spaces and a predatory threat, while also increasing freezing during predator exposure, but not during exposure to a fear conditioned shock grid. Lastly, we show that optogenetic activation of the VMH recruits several regions known to be critical for defensive behaviours, including key hypothalamic and brainstem defensive nodes. These data further support a vital role for VMH *sfl* cells in predator-induced behaviours, in agreement with prior studies.

A recent report has demonstrated that optogenetic activation of the VMH projection to the anterior hypothalamus produces flight (Wang et al., 2015). In agreement with a role for VMH cells in flight, our data show that escape from a predator can be decoded using an unsupervised method (Figure 4h). Furthermore, VMH neural activity could also be used to predict the occurrence of future escape. Considering the prior publication discussed above, it is possible that these escape signals from VMH cells are being conveyed to the anterior hypothalamus to initiate escape. It is also possible that escape signals from the VMH may be transmitted to the dorsal premammillary nucleus, a hypothalamic structure that controls both the occurrence and the vigour of escape response from multiple innate threat modalities (Wang, Schuette, La-Vu, et al., 2021; Wang, Schuette, Nagai, et al., 2021).

Both our data and prior reports indicate that VMH *sfl* cell activation increases freezing (Kunwar et al., 2015; Wang et al., 2015). However, we did not observe consistent activation during or prior to the onset of freezing. This indicates that perhaps only a minority of VMH cells

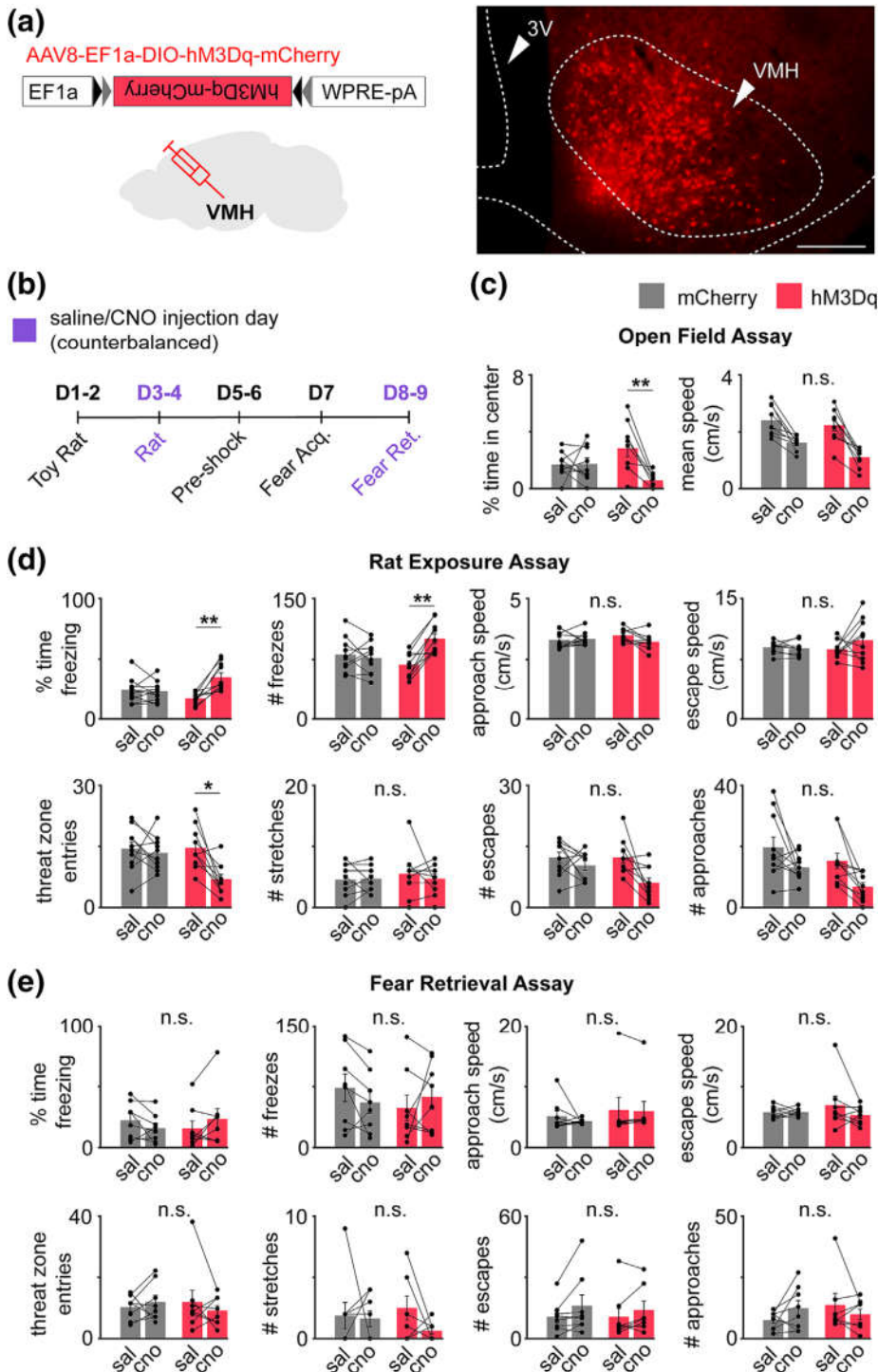


FIGURE 5 (a, left) VMH was targeted with AAV8-EF1a-DIO-hM3Dq-mCherry or AAV8-EF1a-DIO-mCherry. (a, right) Example histology. (b) Mice were exposed to assays in the order shown, after receiving i.p. injections of either saline or CNO for those labelled in purple. (c) Bars show the % time spent in the centre of the open field and mean speed for CNO and saline sessions (two-way repeated measures ANOVA followed by Wilcoxon rank sum test; mCherry $n = 9$, hM3Dq $n = 9$). (d) Excitation hM3Dq-expressing cells in the VMH increased freezing and decreased threat zone entries in the rat exposure assay (two-way repeated measures ANOVA followed by Wilcoxon rank sum test; mCherry $n = 10$, hM3Dq $n = 10$). (e) Excitation of hM3Dq-expressing cells in the VMH had no significant effect for all tested metrics in the fear retrieval assay (two-way repeated measures ANOVA followed by Wilcoxon rank sum test; mCherry $n = 8$, hM3Dq $n = 8$). ** $p < .01$, * $p < .05$

influences freezing. Indeed, we found a small fraction of cells in which neural activity correlated with freezing (Figure 4d). Another possibility is that the recently reported persistent activation of VMH cells following predator exposure may be responsible for encoding freezing.

It is noteworthy that bulk fibre photometry recordings do not show VMH activation prior to or during freezing (Figure 2f). Furthermore, only a small fraction of

cells showed significant correlation of activity with freezing (Figure 5d). These data indicate that VMH does not display prominent activity time-locked to freezing. Consequently, we could not predict the occurrence of freezing using VMH neural activity (Figure 4e). Despite these results, VMH excitation increased freezing during exposure to the predatory rat (Figure 5d). It is possible that the small number of detected cells that correlate with freezing induce freezing but they do so with inconsistent

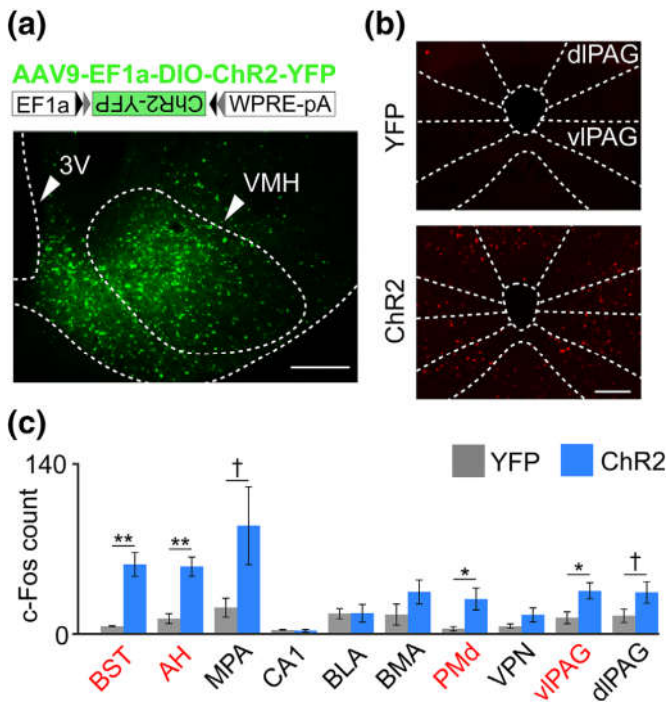


FIGURE 6 (a) Mice were injected with AAV9-EF1a-DIO-ChR2-YFP in the VMH. Image shows expression of Chr2-YFP in VMH cells (scale bar: 150 μ m). (b) Following optogenetic activation of VMH cells, mice were perfused and stained with antibodies against the immediate early gene *cfos*. Representative image shows that blue light delivery caused increased fos expression in the ventrolateral and dorsolateral periaqueductal grey (vIPAG and dIPAG) (scale bar: 150 μ m). (c) Average number of fos-expressing cells in various brain regions following light delivery to Chr2 (blue) or YFP (grey)-expressing cells. Regions for which the *c-Fos* count is significantly greater for Chr2 than YFP mice are labelled in red (two-sample *t* test; Chr2 $n = 4$, YFP $n = 3$). ** $p < .01$, * $p < .05$, † $p < .077$. Abbreviations: BST, bed nucleus of the stria terminalis; AH, anterior hypothalamic nucleus; MPA, medial preoptic area; CA1, CA1 region of the hippocampus; BLA, basolateral amygdala; BMA, basomedial amygdala; PMd, dorsal preammillary nucleus of the hypothalamus; VPN, ventral preammillary nucleus; vIPAG, ventrolateral periaqueductal grey; dIPAG, dorsolateral periaqueductal grey

activity across freezing bouts, and that is why we were unable to predict freezing. Another possibility is that even though there are few freezing correlated cells, perhaps higher VMH activity during the predatory exposure induces a higher defensive state in which freezing is more likely to happen, but the exact timing of the freezing bouts may be determined by activity in downstream targets such as the periaqueductal grey. Indeed, VMH activity has been linked to a persistent state (Kunwar et al., 2015; Wang et al., 2015), and activation of the VMH projection to the periaqueductal grey region induces freezing (Wang et al., 2015). We also note that,

though VMH activity could predict escape, chemogenetic excitation of VMH sf1 cells did not increase the number of escapes. This result occurred because excitation of VMH cells induces a higher defensive state, which enhances avoidance of the rat. Accordingly, VMH excitation decreased the number of entries into the rat threat zone (Figure 5d). Escapes can only happen following approaches near the rat, as the mouse cannot escape if it is already far from the rat. As VMH excitation decreased entries into the threat zone, this manipulation cannot simultaneously also increase the number of escapes. Nevertheless, when escapes were observed, high VMH activation is seen (Figure 4d–f). This is why even though VMH activity is higher during escape, VMH excitation did not increase the number of escapes. Generally, prior studies have shown that VMH inhibition decreased defensive behaviours elicited by either innate threats or predator conditioned contexts (Silva et al., 2013, 2016; Kunwar et al., 2015). These results complement the current data showing that VMH activation increases avoidance of threat.

Previous data using optogenetics have shown that VMH sf1 cell activation produces freezing and escape in an empty open field even in the absence of threats (Kunwar et al., 2015; Wang et al., 2015). Importantly, in an empty open field, we did not observe any freezing or escape jumps in hM3Dq-expressing mice treated with the ligand clozapine-N-oxide. However, chemogenetic activation of VMH cells increased freezing and avoidance of a live predator. The differences between chemogenetic and optogenetic activation suggest that VMH sf1 strong synchronous optogenetic activation may produce results that are not observed with milder asynchronous chemogenetic manipulations.

Intriguingly, the VMH is activated by social threats (Newman et al., 2019), and it encodes spatial location in a context previously paired with a social threat (Krzywkowski et al., 2020). Now, we characterized activation of this same structure during a predatory encounter. These data suggest the tantalizing possibility that the same VMH ensembles may encode both types of threats, though future studies are needed to investigate this view. Our data complement these results and show that the VMH encodes important defensive variables, such as distance to threat. These data complement prior results that also show VMH activity increases during escape from predator and also encodes distance to predator (Esteban Masferrer et al., 2020). One important difference is that this prior report was done with electrodes, allowing higher temporal resolution than calcium imaging. However, calcium imaging allows us to record neural activity with genetic specificity in sf1 VMH cells. Importantly, our data also support prior results, indicating that the

VMH is involved in defensive actions elicited by innate predators (Silva et al., 2013). Our data also show that VMH activation does not change defensive responses during fear retrieval to an environment containing a shock grid. Despite these chemogenetic negative data on shock grid fear retrieval, it is important to highlight that VMH activity is necessary for the acquisition and expression of predator-induced contextual fear memory (Silva et al., 2016). These data indicate that the VMH is not necessary for conditioned fear in general but only for learned fear related to predator exposure.

The VMH has been shown to be involved in the generation of a persistent, scalable defensive state (Kunwar et al., 2015; Kennedy et al., 2020). Accordingly, our data suggest that activation of VMH cells is sufficient to recruit numerous defensive nodes (Figure 6c), in agreement with the view that this region can induce a persistent defensive state. Furthermore, the VMH is well positioned to control such states, as it is a key component of the medial hypothalamic defense system that coordinates threat detection and appropriate defensive behaviours during predatory encounters (Cezario et al., 2008; Martinez et al., 2008; Silva et al., 2013). Taken together, our results thus highlight the role of the VMH in survival behaviours during predatory exposure.

4 | METHODS

All procedures conformed to guidelines established by the National Institutes of Health and have been approved by the University of California, Los Angeles, Institutional Animal Care and Use Committee, protocols 2017-011 and 2017-075.

4.1 | Mice

Sfl-IRES-Cre mice (Jackson Laboratory Stock No. 033687) were used for all experiments. Male and female mice between 13 and 17 weeks of age were used in all experiments. For fibre photometry and miniaturized microscope experiments, mice were between 13 and 15 weeks. For miniaturized microscope recordings, mice were between 14 and 16 weeks. For chemogenetic excitation experiments, all mice were between 15 and 17 weeks. Mice were maintained on a 12-h reverse light–dark cycle with food and water ad libitum. Sample sizes were chosen based on previous behavioural optogenetics studies on defensive behaviours. All mice were handled for a minimum of 5 days prior to any behavioural task. Exclusion criteria were animal sickness or mis-targeted viral expression. No surgicized mice were excluded,

except for one mouse that did not recuperate well from the surgery and remained lethargic for several days.

4.2 | Rats

Male Long-Evans rats (250–400 g) were obtained from Charles River Laboratories and were individually housed on a standard 12-h light–dark cycle and given food and water ad libitum. Rats were only used as a predatory stimulus. Rats were handled for several weeks prior to being used and were screened for low aggression to avoid attacks on mice. No attacks on mice were observed in this experiment.

4.3 | Viral vectors

All vectors were purchased from Addgene.

- Optogenetics: AAV9-EF1a-DIO-hChR2(H134R)-eYFP, WPRE-hGH and AAV9-EF1a-DIO-eYFP.
- Chemogenetics: pAAV8-hSyn-DIO-hM4D(Gi)-mCherry and AAV8-Syn-DIO-mCherry.
- Fibre photometry and miniaturized microscope recordings: AAV9-Syn-FLEX-GCaMP6s-WPRE-SV40.

4.4 | Surgeries

Surgeries were performed as described previously (Adhikari et al., 2015). Eight-week-old mice were anaesthetized with 1.5–3.0% isoflurane and placed in a stereotaxic apparatus (Kopf Instruments). A scalpel was used to open an incision along the midline to expose the skull. After performing a craniotomy, 40 nl of one of the viral vectors listed above at a titre of 2×10^{12} particles/ml was injected per site (VMH) using a 10 μ l nanofil syringe (World Precision Instruments) at 0.08 μ l/min. All viruses were injected at a titre of 2×10^{12} particles/ml. The syringe was coupled to a 33-gauge bevelled needle, and the bevel was placed to face the anterior side of the animal. The syringe was slowly retracted 20 min after the start of the infusion. Mice received unilateral viral infusion and fibre optic cannula implantation. Infusion locations measured in millimetres as anterior–posterior, medial–lateral and dorso–ventral coordinates from bregma were VMH (–1.46, 0.5, 5.5).

For optogenetic experiments, the fibre optic cannula (0.22 numerical aperture, 200 μ m diameter; Newdoon) was implanted unilaterally 0.15 mm above the viral infusion site. Only mice with viral expression restricted to the intended targets were used for behavioural assays.

For photometry experiments, mice were implanted unilaterally with fibreoptic cannulae in the VMH. A 400 μm diameter, 0.48 NA optical fibre (Neurophotometrics) was used for photometry experiments. Adhesive cement (C&B metabond; Parkell, Edgewood, NY, USA) and dental cement (Stoelting, Wood Dale, IL, USA) were used to securely attach the fibre optic cannula to the skull. For miniaturized microscope experiments, 40 nl of AAV9-DIO-GCaMP6s was injected in the VMH of *sf1-cre* mice, and a 7 mm GRIN lens was implanted 200 μm above the infusion site. Three weeks following surgery, animals were base-plated. Brain hemispheres were counterbalanced across mice for fibre photometry and miniaturized microscope surgeries.

4.5 | Rat exposure assay

Mice were accustomed to handling prior to any behavioural assay. On day 1, mice were habituated to a rectangular box (70 cm length, 26 cm width, 44 cm height) for 20 min. This environment consisted of a large aquarium made of glass. Sheets of paper lined the outside glass surface. The box was cleaned with ethanol between mice. Twenty-four hours later, mice were exposed to the same environment but in the presence of a toy rat for 20 min. Mice were then exposed to an adult rat or a toy rat in this environment on the two following days. The rat was secured by a harness tied to one of the walls and could freely ambulate only within a short radius of approximately 20 cm. The mouse was placed near the wall opposite to the rat and freely explored the context for 20 min. No separating barrier was placed between the mouse and the rat, allowing for close naturalistic encounters that can induce a variety of robust defensive behaviours.

4.6 | Contextual fear conditioning test

To better evaluate a broader species-specific defense repertoire in face of a conditioned stimulus, we used a modified version of the standard contextual fear conditioning method (Schuette et al., 2020). Pre-shock, fear conditioning and retrieval sessions were performed in a context (70 cm length \times 17 cm width \times 40 cm height) with an evenly distributed light intensity of 40 lux and a Coulbourn shock grid (19.5 cm \times 17 cm) set at the extreme end of the enclosure. The fear conditioning environment is made of laminated white foam board. The box was cleaned with ethanol between mice. Forty-eight hours after rat exposure, mice were habituated to this context and could freely explore the whole environment for 20 min. On the following day, the grid was activated, such

that a single 0.7 mA foot shock was delivered for 2 s only on the first time the mouse fully entered the grid zone. Twenty-four hours later, retrieval sessions were performed in the same enclosure but without shock. Mice could freely explore the context for 20 min during pre-shock habituation, fear conditioning and retrieval sessions.

4.7 | Behavioural quantification

To extract the pose of freely behaving mice in the described assays, we implemented DeepLabCut (Nath et al., 2019), an open-source convolutional neural network-based toolbox, to identify mouse nose, ear and tail base *xy*-coordinates in each recorded video frame. These coordinates were then used to calculate velocity and position at each time point and classify behaviours such as escape runs and freezes in an automated manner using custom Matlab scripts. Specifically:

‘Escapes’ were defined as epochs for which (1) the mouse speed away from the threat or control threat exceeded 2 cm/s (as there was little room for acceleration between the threat zone and opposite wall, the speed threshold was set to this relatively low value.); (2) movement away from the threat was initiated at a minimum distance-from-threat of 30 cm and (3) the distance traversed from escape onset to offset was greater than 10 cm. Thus, escapes were required to begin near the threat and lead to a substantial increase in distance from the threat.

‘Escape speed’ was defined as the average speed from escape onset to offset.

‘Approaches’ were defined as epochs for which (1) the mouse speed towards the threat or control threat exceeded 2 cm/s and (2) the distance traversed from approach onset to offset was greater than 10 cm.

‘Stretch-attend postures’ were defined as epochs for which (1) the distance between mouse nose and tail base exceeded a distance of approximately 1.2 mouse body lengths and (2) mouse tail base speed fell below 1 cm/s.

‘Freezes’ were defined as periods for which mouse nose and tail base speed fell below 0.25 cm/s for at least 0.33 s (Schuette et al., 2020). ‘Freeze bout duration’ was defined as the amount of time that elapsed from freeze onset to offset.

All behaviours were manually checked by the experimenters for error.

4.8 | Order and schedule of behavioural assays

First, all mice, used for either chemogenetics or neural activity recordings, were habituated to handling for

5 days. All behavioural sessions lasted 20 min for all assays, with the exception of the 10-min open field session. No differences were observed between male and female mice in any of the assays (Figures S1 and S3).

For mice used in miniscope and fibre photometry recordings, following handling habituation, mice were exposed to the open field for 10 min (day 1). Then, mice were habituated to the rat enclosure for 20-min sessions for 2 days (days 2–3). The toy rat and live rat were introduced on days 4 and 5, respectively. This was followed by habituation to the fear conditioning enclosure on day 6 (this was the pre-shock control session). Fear acquisition and retrieval were performed, respectively, on days 7 and 8.

For mice used in chemogenetics, the same order of assays was used. Mice were exposed to each environment twice, with treatment of either CNO or saline. Saline or 5 mg/kg CNO was administered on contiguous days counterbalanced across mice. Open field was done on days 1 and 2. Habituation to the rat enclosure occurred on days 2–4. The toy rat was introduced on days 4 and 5 (each day with CNO or saline treatment) and the live rat on days 8 and 9 (also with CNO or saline treatment). This was followed by habituation to the fear conditioning enclosure on days 11–13. Day 14 was the pre-shock session. Fear acquisition occurred on day 15, followed by fear retrieval on days 17 and 18 (CNO or saline treatment on each day).

4.9 | Fibre photometry

Photometry was performed as described in detail previously (Kim et al., 2016). Briefly, we used a 405-nm LED and a 470-nm LED (Thorlabs, M405F1 and M470F1) for the Ca^{2+} -dependent and Ca^{2+} -independent isosbestic control measurements. The two LEDs were bandpass filtered (Thorlabs, FB410-10 and FB470-10) and then combined with a 425-nm longpass dichroic mirror (Thorlabs, DMLP425R) and coupled into the microscope using a 495-nm longpass dichroic mirror (Semrock, FF495-Di02-25 × 36). Mice were connected with a branched patch cord (400 μm , Doric Lenses, Quebec, Canada) using a zirconia sleeve to the optical system. The signal was captured at 20 Hz (alternating 405-nm LED and 470-nm LED). To correct for signal artefacts of a non-biological origin (i.e., photobleaching and movement artefacts), custom Matlab scripts leveraged the reference signal (405 nm), unaffected by calcium saturation, to isolate and remove these effects from the calcium signal (470 nm). The $\text{d}f/F$ was calculated in this manner across the entire recording session before any additional analyses, such as behavioural averaging, were performed.

No further filtering was applied to the signal. Sample code and data is available online (at github.com/schuettepeter/FiberPhotometryExtraction).

4.10 | Fibre photometry behaviour-triggered averaging

To plot the behaviour-triggered averages, only mice that displayed a minimum of three behavioural instances were included in the corresponding behavioural figure. Moreover, event-triggered averages were only calculated from behavioural instances that were separated from other classified behavioural instances by a minimum of 5 s.

4.11 | Miniscope video capture

All videos were recorded at 30 frames per second using a Logitech HD C310 webcam and custom-built head-mounted UCLA miniscope (Cai et al., 2016). Open-source UCLA Miniscope software and hardware (miniscope.org/) were used to capture and synchronize neural and behavioural video (Cai et al., 2016).

4.12 | Miniscope postprocessing

The open-source UCLA miniscope analysis package (github.com/daharoni/Miniscope_Analysis) (Aharoni & Hoogland, 2019) was used to motion correct miniscope videos. They were then temporally down sampled by a factor of 4 and spatially down sampled by a factor of 2. The cell activity and footprints were extracted using the open-source package Constrained Nonnegative Matrix Factorization for microEndoscopic data (CNMF-E; github.com/zhoup/CNMF_E) (Schuette et al., 2020; Zhou et al., 2018). Only cells whose variance was greater than or equal to 25% of the maximum variance among non-outliers were used in the analysis.

4.13 | Behaviour cell classification

We used a GLM to identify cells that showed increased calcium activity during approach, stretch-attend, escape and freeze behaviours. We fit this model to each cell's activity, with behaviour indices as the predictor variable and behaviour coefficients as the measure of fit. Neural data were circularly shifted by equal increments over 100 iterations, and a bootstrap distribution was built from the resulting GLM coefficients. A cell was considered a

behaviour-categorized cell if its actual coefficient exceeded 95% of the bootstrap coefficient values.

4.14 | Behaviour decoding using VMH neural data

Discrete classification of escape behaviour was performed using multinomial logistic regression. Time points following escape by 2 s were labelled 'escape,' and a matched number of non-escape time points were randomly selected for training and validation. Each time point was treated as an individual data point. Training and validation were performed using fivefold cross-validation, with a minimum of 10 s between training and validation sets. As equal numbers of escape and non-escape samples were used to build the training and validation sets, chance accuracy was 50%. Sessions with less than five escapes were excluded from the analysis. The same analysis was performed for approach, stretch-attend postures and freeze. To predict escape at negative time lags from behaviour onset, the same analysis procedure was implemented, using 2-s epochs preceding escape by 2, 4, 6, 8 and 10 s.

4.15 | K-means clustering

The unsupervised k-means algorithm was used to separate the VMH ensemble activity into two states. The only inputs to the model were the top principal components of the neural data (accounting for $\geq 80\%$ of the total variance). No behavioural information was provided to the model. The cluster with the most corresponding escapes was labelled the 'escape cluster'. All sessions for each assay were concatenated, and accuracy was calculated as the percent of escape indices to co-occur with this escape state. To determine chance level, we built a bootstrapped distribution of accuracies (1,000 iterations), randomly selecting indices (the same number as escape indices) and calculating the percent that co-occurred with the escape cluster by chance. Chance level was defined as the 95th percentile of the resulting distribution.

4.16 | Chemogenetics

Mice used for chemogenetic experiments were exposed to each threat and control stimuli twice, once following treatment with saline and once following treatment with CNO (5 mg/kg, injected intraperitoneally) 40 min prior to the experiment. Only one control or threat-exposure assay was performed per day with each mouse.

4.17 | Behaviour video capture

All behaviour videos were captured at 30 frames per second in standard definition (640 × 480) using a Logitech HD C310 webcam. To capture fibre-photometry synchronized videos, both the calcium signal and behaviour were recorded by the same computer using custom Matlab scripts that also collected timestamp values for each calcium sample/behavioural frame. These timestamps were used to precisely align neural activity and behaviour.

4.18 | Induction of cfos expression by optogenetic activation

Mice were first habituated to handling for 5 days, in 10-min daily sessions. Blue light was generated by a 473 nm laser (Dragon Lasers, Changchun Jilin, China) at 5.0 mW unless otherwise indicated. A Master-8 pulse generator (A.M.P.I., Jerusalem, Israel) was used to drive the blue laser at 20 Hz, using 5-ms pulses. The laser output was delivered to the animal via an optical fibre (200 μm core, 0.22 numerical aperture, Doric Lenses, Canada) coupled to the fiberoptic implanted on the animals through a zirconia sleeve. Mice received optogenetic stimulation with these parameters for 10 min in a grey open field following habituation handling. Mice then rested in their homecage for 90 min to allow for expression of cfos protein, and then, they were perfused as described below.

4.19 | Perfusion and histological verification

Mice were anaesthetized with Fatal-Plus and transcardially perfused with phosphate buffered saline followed by a solution of 4% paraformaldehyde. Extracted brains were stored for 12 h at 4°C in 4% paraformaldehyde. Brains were then placed in sucrose for a minimum of 24 h. Brains were sectioned in the coronal plane in a cryostat, washed in phosphate buffered saline and mounted on glass slides using PVA-DABCO. Images were acquired using a Keyence BZ-X fluorescence microscope with a 10X or 20X air objective.

4.20 | Immunostaining and quantification for cfos

Fixed brains were kept in 30% sucrose at 4°C overnight and then sectioned on a cryostat (40 μm) slices. Sections were washed in PBS and incubated in a blocking solution

(3% normal donkey serum and 0.3% triton-x in PBS) for 1 h at room temperature. Sections were then incubated at 4°C for 12 h with polyclonal anti-fofos antibody made in rabbit (1/500 dilution) (c-Fos [9F6] Rabbit mAb CAT#2250, Cell Signaling Technology) in blocking solution. Following primary antibody incubation, sections were washed in PBS 3 times for 10 min and then incubated with anti-rabbit IgG (H + L) antibody (1/500 dilution) conjugated to Alexa Fluor 594 (red) (CAT# 8889S, cellsignal.com) for 1 h at room temperature. Sections were washed in PBS three times for 10 min, incubated with DAPI (1/50,000 dilution in PBS), washed again in PBS and mounted in glass slides using PVA-DABCO (Sigma). Sections were imaged at 10X magnification using a ZEISS LSM 900 confocal microscope. Images of the VMH were collected to record green (GFP-expressing VMH sf1 cells) and red (cFos-expressing cells) fluorescence. For each animal, images were quantified using ImageJ software (National Institutes of Health). In each mouse, cFos expressing cells were counted in three representative fields of view in each region of interest. Data were first averaged across fields of view for each mouse and then averaged across mice.

4.21 | Statistical analysis

All statistical analyses were performed using custom Matlab scripts. Nonparametric Wilcoxon signed-rank or rank-sum tests were used, unless otherwise stated. Two-tailed tests were used throughout with $\alpha = .05$. Asterisks in the figures indicate the p values. Standard error of the mean was plotted in each figure as an estimate of variation. Multiple comparisons were adjusted with the false discovery rate method.

AUTHOR CONTRIBUTIONS

Brooke C Tobias: Conceptualization; investigation; methodology. **Peter J Schuette:** Formal analysis; software; visualization. **Sandra Maesta-Pereira:** Formal analysis; software; visualization. **Anita Torossian:** Investigation. **Weisheng Wang:** Investigation. **Ekayana Sethi:** Investigation. **Avishek Adhikari:** Conceptualization; resources; supervision; writing - original draft; writing - review and editing.

ACKNOWLEDGEMENTS

We were supported by the National Institute of Mental Health (R00 MH106649 and R01 MH119089 to A.A.), the Brain and Behavior Research Foundation (22663 and 27780 to A.A. and W.W., respectively); the National Science Foundation (NSF-GRFP DGE-1650604 to P.S.); the UCLA Affiliates Fellowship (to P.S.) and the Hellman

Foundation (to A.A.). We thank H.T. Blair and K.M. Wassum for providing the rats.

CONFLICT OF INTEREST

The authors declare no competing interests.

DATA AVAILABILITY STATEMENT


Data are available from A.A. upon request.

PEER REVIEW

The peer review history for this article is available at <https://publons.com/publon/10.1111/ejn.15937>.

ORCID

Sandra Maesta-Pereira  <https://orcid.org/0000-0001-6522-8311>

Avishek Adhikari  <https://orcid.org/0000-0002-9187-9211>

REFERENCES

- Adhikari, A., Lerner, T. N., Finkelstein, J., Pak, S., Jennings, J. H., Davidson, T. J., Ferenczi, E., Gunaydin, L. A., Mirzabekov, J. J., Ye, L., Kim, S.-Y., Lei, A., & Deisseroth, K. (2015). Basomedial amygdala mediates top-down control of anxiety and fear. *Nature*, *527*, 179–185. <https://doi.org/10.1038/nature15698>
- Aharoni, D., & Hoogland, T. M. (2019). Circuit investigations with open-source miniaturized microscopes: Past, present and future. *Frontiers in Cellular Neuroscience*, *13*, 141. <https://doi.org/10.3389/fncel.2019.00141>
- Beitz, A. J. (1982). The organization of afferent projections to the midbrain periaqueductal gray of the rat. *Neuroscience*, *7*, 133–159. [https://doi.org/10.1016/0306-4522\(82\)90157-9](https://doi.org/10.1016/0306-4522(82)90157-9)
- Cai, D. J., Aharoni, D., Shuman, T., Shobe, J., Biane, J., Song, W., Wei, B., Veshkini, M., La-Vu, M., Lou, J., Flores, S. E., Kim, I., Sano, Y., Zhou, M., Baumgaertel, K., Lavi, A., Kamata, M., Tuszyński, M., Mayford, M., ... Silva, A. J. (2016). A shared neural ensemble links distinct contextual memories encoded close in time. *Nature*, *534*, 115–118. <https://doi.org/10.1038/nature17955>
- Canteras, N. S., & Swanson, L. W. (1992). The dorsal premammillary nucleus—An unusual component of the mammillary body. *Proceedings of the National Academy of Sciences of the United States of America*, *89*, 10089–10093. <https://doi.org/10.1073/pnas.89.21.10089>
- Cezario, A. F., Ribeiro-Barbosa, E. R., Baldo, M. V., & Canteras, N. S. (2008). Hypothalamic sites responding to predator threats—The role of the dorsal premammillary nucleus in unconditioned and conditioned antipredatory defensive behavior. *European Journal of Neuroscience*, *28*, 1003–1015. <https://doi.org/10.1111/j.1460-9568.2008.06392.x>
- Comoli, E., Ribeiro-Barbosa, E. R., & Canteras, N. S. (2000). Afferent connections of the dorsal premammillary nucleus. *Journal of Comparative Neurology*, *423*, 83–98. [https://doi.org/10.1002/1096-9861\(20000717\)423:1<83::aid-cne7>3.0.co;2-3](https://doi.org/10.1002/1096-9861(20000717)423:1<83::aid-cne7>3.0.co;2-3)
- Esteban Masferrer, M., Silva, B. A., Nomoto, K., Lima, S. Q., & Gross, C. T. (2020). Differential encoding of predator fear in

- the ventromedial hypothalamus and periaqueductal grey. *Journal of Neuroscience*, 40, 9283–9292. <https://doi.org/10.1523/JNEUROSCI.0761-18.2020>
- Faturi, C. B., Rangel, M. J. Jr., Baldo, M. V., & Canteras, N. S. (2014). Functional mapping of the circuits involved in the expression of contextual fear responses in socially defeated animals. *Brain Structure and Function*, 219, 931–946. <https://doi.org/10.1007/s00429-013-0544-4>
- Kennedy, A., Kunwar, P. S., Li, L.-Y., Stagkourakis, S., Wagenaar, D. A., & Anderson, D. J. (2020). Stimulus-specific hypothalamic encoding of a persistent defensive state. *Nature*, 586, 730–734. <https://doi.org/10.1038/s41586-020-2728-4>
- Kim, C. K., Yang, S. J., Pichamoorthy, N., Young, N. P., Kauvar, I., Jennings, J. H., Lerner, T. N., Berndt, A., Lee, S. Y., Ramakrishnan, C., Davidson, T. J., Inoue, M., Bito, H., & Deisseroth, K. (2016). Simultaneous fast measurement of circuit dynamics at multiple sites across the mammalian brain. *Nature Methods*, 13, 325–328. <https://doi.org/10.1038/nmeth.3770>
- Krzywkowski, P., Penna, B., & Gross, C. T. (2020). Dynamic encoding of social threat and spatial context in the hypothalamus. *eLife*, 9, e57148. <https://doi.org/10.7554/eLife.57148>
- Kunwar, P. S., Zelikowsky, M., Remedios, R., Cai, H., Yilmaz, M., Meister, M., & Anderson, D. J. (2015). Ventromedial hypothalamic neurons control a defensive emotion state. *eLife*, 4, e06633. <https://doi.org/10.7554/eLife.06633>
- Martinez, R. C., Carvalho-Netto, E. F., Amaral, V. C., Nunes-de-Souza, R. L., & Canteras, N. S. (2008). Investigation of the hypothalamic defensive system in the mouse. *Behavioral Brain Research*, 192, 185–190. <https://doi.org/10.1016/j.bbr.2008.03.042>
- Nath, T., Mathis, A., Chen, A. C., Patel, A., Bethge, M., & Mathis, M. W. (2019). Using DeepLabCut for 3D markerless pose estimation across species and behaviors. *Nature Protocols*, 14, 2152–2176. <https://doi.org/10.1038/s41596-019-0176-0>
- Newman, E. L., Covington, H. E. 3rd, Suh, J., Bickacsi, M. B., Ressler, K. J., DeBold, J. F., & Miczek, K. A. (2019). Fighting females: Neural and behavioral consequences of social defeat stress in female mice. *Biological Psychiatry*, 86, 657–668. <https://doi.org/10.1016/j.biopsych.2019.05.005>
- Perusini, J. N., & Fanselow, M. S. (2015). Neurobehavioral perspectives on the distinction between fear and anxiety. *Learning and Memory*, 22, 417–425. <https://doi.org/10.1101/lm.039180.115>
- Schuetz, P. J., Reis, F. M. C. V., Maesta-Pereira, S., Chakerian, M., Torossian, A., Blair, G. J., Wang, W., Blair, H. T., Fanselow, M. S., Kao, J. C., & Adhikari, A. (2020). Long-term characterization of hippocampal remapping during contextual fear acquisition and extinction. *Journal of Neuroscience*, 40, 8329–8342. <https://doi.org/10.1523/JNEUROSCI.1022-20.2020>
- Silva, B. A., Mattucci, C., Krzywkowski, P., Cuzzo, R., Carbonari, L., & Gross, C. T. (2016). The ventromedial hypothalamus mediates predator fear memory. *European Journal of Neuroscience*, 43, 1431–1439. <https://doi.org/10.1111/ejn.13239>
- Silva, B. A., Mattucci, C., Krzywkowski, P., Murana, E., Illarionova, A., Grinevich, V., Canteras, N. S., Ragozzino, D., & Gross, C. T. (2013). Independent hypothalamic circuits for social and predator fear. *Nature Neuroscience*, 16, 1731–1733. <https://doi.org/10.1038/nn.3573>
- Wang, L., Chen, I. Z., & Lin, D. (2015). Collateral pathways from the ventromedial hypothalamus mediate defensive behaviors. *Neuron*, 85, 1344–1358. <https://doi.org/10.1016/j.neuron.2014.12.025>
- Wang, W., Schuetz, P. J., La-Vu, M. Q., Torossian, A., Tobias, B. C., Ceko, M., Kragel, P. A., Reis, F. M., Ji, S., Sehgal, M., Maesta-Pereira, S., Chakerian, M., Silva, A. J., Canteras, N. S., Wager, T., Kao, J. C., & Adhikari, A. (2021). Dorsal premammillary projection to periaqueductal gray controls escape vigor from innate and conditioned threats. *eLife*, 10, e69178. <https://doi.org/10.7554/eLife.69178>
- Wang, W., Schuetz, P. J., Nagai, J., Tobias, B. C., Cuccovia, V., Reis, F. M., Ji, S., de Lima, M. A. X., La-Vu, M. Q., Maesta-Pereira, S., Chakerian, M., Leonard, S. J., Lin, L., Severino, A. L., Cahill, C. M., Canteras, N. S., Khakh, B. S., Kao, J. C., & Adhikari, A. (2021). Coordination of escape and spatial navigation circuits orchestrates versatile flight from threats. *Neuron*, 109, 1848–1860.e8. <https://doi.org/10.1016/j.neuron.2021.03.033>
- Xie, Z., Gu, H., Huang, M., Cheng, X., Shang, C., Tao, T., Li, D., Xie, Y., Zhao, J., Lu, W., Zhang, Z., Zhan, C., Tang, Z., Zhang, F., & Cao, P. (2022). Mechanically evoked defensive attack is controlled by GABAergic neurons in the anterior hypothalamic nucleus. *Nature Neuroscience*, 25, 72–85. <https://doi.org/10.1038/s41593-021-00985-4>
- Zhang, J., Chen, D., Sweeney, P., & Yang, Y. (2020). An excitatory ventromedial hypothalamus to paraventricular thalamus circuit that suppresses food intake. *Nature Communications*, 11, 6326. <https://doi.org/10.1038/s41467-020-20093-4>
- Zhou, P., Resendez, S. L., Rodriguez-Romaguera, J., Jimenez, J. C., Neufeld, S. Q., Giovannucci, A., Friedrich, J., Pnevmatikakis, E. A., Stuber, G. D., Hen, R., Kheirbek, M. A., Sabatini, B. L., Kass, R. E., & Paninski, L. (2018). Efficient and accurate extraction of in vivo calcium signals from microendoscopic video data. *eLife*, 7, e28728. <https://doi.org/10.7554/eLife.28728>

SUPPORTING INFORMATION

Additional supporting information can be found online in the Supporting Information section at the end of this article.

How to cite this article: Tobias, B. C., Schuetz, P. J., Maesta-Pereira, S., Torossian, A., Wang, W., Sethi, E., & Adhikari, A. (2023). Characterization of ventromedial hypothalamus activity during exposure to innate and conditioned threats. *European Journal of Neuroscience*, 57(7), 1053–1067. <https://doi.org/10.1111/ejn.15937>